

Chapter 2

Ions Responsive Asymmetric Conical Shaped Single Nanochannel

2.1 Introduction

Potassium is especially crucial in modulating the activity of muscles and nerves, cells of which have specialized ion channels for transporting potassium. Normal body function extremely depends on the regulation of potassium concentrations inside the ion channels within a certain range. For life science, undoubtedly, it is significant and challenging to study and imitate these processes happening in living organisms with a convenient artificial system. In this chapter, I introduce a novel biomimetic nanochannel system which has an ion concentration effect that provides a nonlinear response to potassium ion at the concentration ranging from 0 to 1500 μM [1]. This new phenomenon is caused by the G-quadruplex (G4) DNA conformational change with a positive correlation with ion concentration. In this work, G4 DNA was immobilized onto a synthetic nanochannel, which undergoes a potassium-responsive conformational change and then induces the change in the effective channel size. The responsive ability of this system can be regulated by the stability of G4 structure through adjusting potassium concentration. The situation of the grafting G4 DNA on a single nanochannel can closely imitate the *in vivo* condition because the G-rich telomere overhang is attached to the chromosome. Therefore, this artificial system could promote a potential to conveniently study biomolecule conformational change in confined space by the current measurement, which is significantly different from the nanopore sequencing. Moreover, such a system may also potentially spark further experimental and theoretical efforts to simulate the process of ion transport in living organisms and can be further generalized to other more complicated functional molecules for the exploitation of novel bio-inspired intelligent nanochannel machines.

Inspired by the biological ion channel, a synthetic film with a single nanochannel structure was prepared as described by Apel et al. [2]. Unlike the fragile lipid-bilayer membrane in which most natural ion channels are embedded, this synthetic film is mechanically and chemically robust. Recently, Martin and Siwy

et al. [3, 4]. reported DNA-nanotube artificial ion channels systems which helped us to better understand the role of an electromechanical gate which responds to the applied voltage, and they also developed the function of this system with DNA single-base mismatch selectivity. J.E ten Elshof et al. reported a system using the nanometer-sized pores of membrane gates to achieve the surfactant-modulated switching of molecular transport [5]. Letant et al. reported localized functionalization of single nanopores [6]. Bashir et al. developed solid-state nanopore channels with DNA selectivity [7]. Jiang et al. reported the gating of single synthetic nanochannels by proton-driven DNA molecular motors [8]. Azzaroni and Ali et al. reported supramolecular bioconjugation in single nanochannel as a biosensor and the

pH-tunable rectifying characteristics of the single conical nanochannels [9–11]. Although ion channels in living organism have been studied by a mimic method using synthetic nanochannels during the past several decades, how to endow these synthetic nanochannels with intelligence is still a challenging task.

In this work, I further extend the function molecules-nanochannel system by using G4 DNA [12–19]. In this biomimetic nanochannel system (BNCS), there is an ion concentration effect, which is a very important phenomenon in living body while other systems do not have. This system is also different from the previous systems [3] utilized the different chain length of non-responsive DNA oligomers, which chemisorbed on the channel walls and surface of the membrane. According to the pH influences on the nanochannel, the previous work about pH responsive i-motif DNA-nanochannel system focused on the permeability ratios of the single nanochannel between two different pH values [8]. The present work is different, because this novel biomimetic nanochannel system was responsive to potassium ion (K^+) within a certain concentration range and simulated these processes in pH neutral environment as in a natural organism [20].

G-quadruplexes are highly ordered DNA structures derived from G-rich sequences formed by tetrads of hydrogen-bonded guanine bases. Among the quadruplex-forming sequences, the human telomeric sequence d[AGGG (TTAGGG)₃] has attracted tremendous interest due to its importance at telomere maintenance and cell aging or death [14]. Recently, there are many researches on the conformational change of this biomolecule [16, 18, 21–23] and its applications in artificial ion channels [24–29] and biosensors [30–33]. Here we selected the G-rich human telomere strand [12, 13, 22, 34] due to the possibility of forming the intramolecular four-stranded quadruplex topologies, and this process is dependent on the alkali metal ion concentration. Considering the efficiency at stabilizing G4 DNA, K^+ is much more effective than other alkali metal ions in promoting the formation of the G4 structures, whereas lithium ion (Li^+) is ineffective in all cases [16, 35]. Therefore, these two ions mentioned above were selected as control to investigate the ion responsive properties of the BNCS.

We prepared a single nanochannel membrane with the well-developed ion-track-etching technique [36–39]. The nanochannel (Fig. 1.6) was embedded in a track-etched polyethylene terephthalate membrane (PET, Hostaphan RN12 Hoechst, 12 μm thick, with single ion track in the center). The track-etching technique

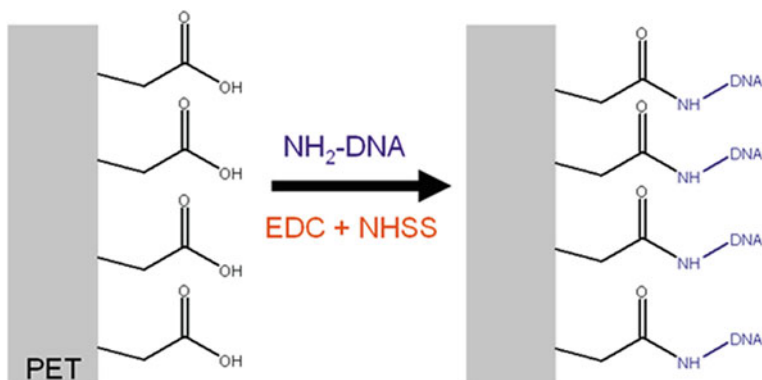


Fig. 2.1 Immobilization of G4 DNA onto the inner wall of the nanochannel by a two-step chemical reaction. Reprinted with the permission from Ref. [1]. Copyright 2009 American Chemical Society

allows control over the shape of the channels, and in this work the etched single nanochannel is cone-like. Diameter measurement of the single conical nanochannel was conducted with a commonly used electrochemical method [37, 39]. Its wide opening (base) is usually several hundred nanometers, and narrow opening (tip) is ~ 20 nm. During the etching process, negatively charged carboxyl groups, which were attached to flexible polymer chains, were created on the channel surface. Then, the amino single-stranded G4 DNA was immobilized onto the inner wall of the nanochannel by a two-step chemical reaction [8] (Fig. 2.1). After grafting G4 DNA on a conical nanochannel wall, the DNA underwent a potassium-responsive conformational change between a random single-stranded structure (without presence of K^+) and a four-stranded G4 structure (with presence of K^+), as shown in Fig. 2.2a, b. This conformational conversion could well induce a change in the effective channel size of the nanochannel, and thus realized K^+ -responsive ion transport properties of the BNCS.

2.2 Materials and Methods

2.2.1 Materials

See Tables 2.1 and 2.2.

2.2.2 Instruments

See Table 2.3.

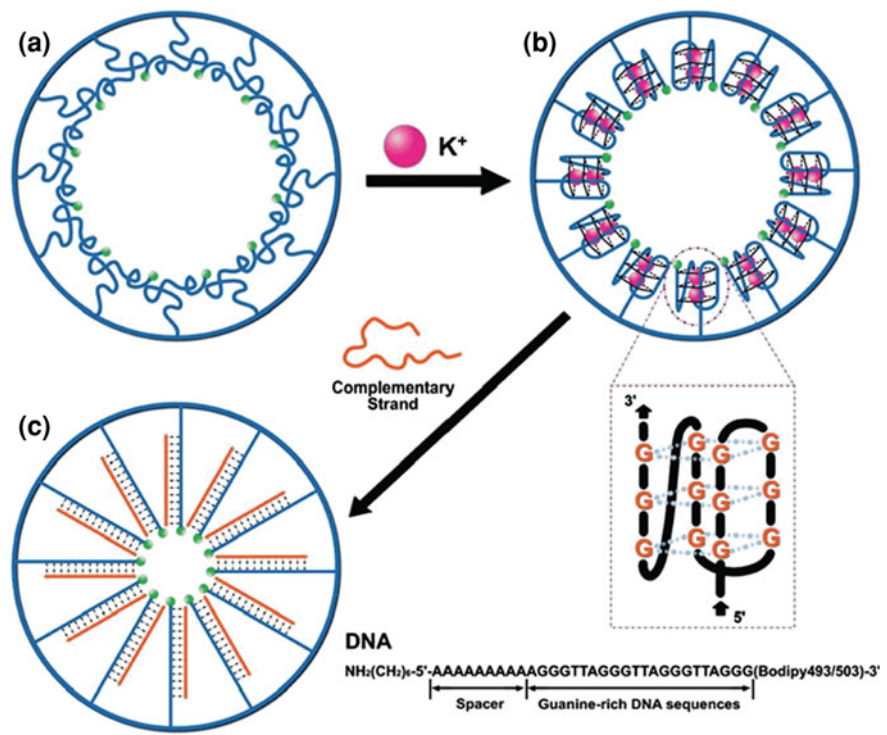


Fig. 2.2 G4 DNA was immobilized onto the inner surface of a single nanochannel. **a** There is no K⁺; the G4 DNA relaxes to a loosely packed single-stranded structure. **b** Presence of K⁺; the G4 DNA folds into densely packed rigid quadruplex structures that partially decrease the effective channel size of the nanochannel. **c** After adding complementary DNA strands, G4 DNA forms a closely packed arrangement of double-stranded DNA on the single nanochannel. Before modification, the etched funnel-shaped single nanochannels are around 20 nm wide at the narrowest point. Reprinted with the permission from Ref. [1]. Copyright 2009 American Chemical Society

Table 2.1 Samples used in the experiments

Sample	Purity and related parameters	Provider
Polyethylene terephthalate (PET) membrane	12 μm thick, with single ion track in the center	GSI, Germany
PET membrane	12 μm thick, with multi-ions track in the center (10 ⁷ /cm ²)	
PET membrane	12 μm thick, without any treatment	Hostaphan RN12 Hoechst, Germany
DNA probe (our design)	HPLC	TAKARA Biotechnology
Primed DNA (our design)	PAGE	(DaLian) Co., Ltd., China

Table 2.2 Reagents used in the experiments

Reagent	Purity quotient	Provider
KCl	A.R.	Beijing Chemical Works
LiCl	A.R.	Beijing Yili Fine Chemical Co., Ltd.
HCl	A.R.	Beijing Chemical Works (Contents 36–38 %)
Tris	A.R.	Made in China
NaOH	A.R.	Beijing Chemical Works
HCOOH	A.R.	Beijing Chemical Works (Contents >88 %)
EDC	≥99.0 % AT	Fluka
NHSS	≥98.5 % HPLC	Fluka
Filamentary silver	99.99 %	Made in China
Platinum filament	99.99 %	Made in China

Table 2.3 Instruments used in the experiments

Instrument	Producer
Water purification system (water, 18.2 MΩ)	Milli-Q, Millipore Corporation, USA
KEITHLEY 6487 picoammeter	Keithley Instruments, Cleveland, OH, USA
ZF-7 Uviol lamp	Shanghai Gucun Optic Instrument Factory, China
Model PHS-25 pH meter instruction	Shanghai Precision & Scientific Instrument Co. Ltd
Jasco J-810 circular dichroism (CD) spectropolarimeter	JASCO Corporation, Japan
Field emission scanning electron microscope, JSM-6700F	JEOL, Japan
X-ray photoelectron spectroscopy, ESCALab220i-XL	Thermo VG Scientific Ltd., UK
Homemade PTFE electrolyzer	ICCAS, China
Homemade plexiglass electrolyzer	ICCAS, China
Hot plate clarkson H3400-HS07	IKA, USA
Stopwatch timer	Made in China
Electronic thermometer	Made in China

2.2.3 Solvent Preparation

Track etching solution for the nanochannel preparation: 9 M NaOH

Stopping solution for the etching solution: 1 M KCl + 1 M HCOOH

CD test solution: Tris (5 mM) + HCl (4.5 mM) + DNA (1 μM)

Transmembrane current test solution:

Tris (5 mM) + HCl (4.5 mM) + KCl or LiCl (0–1500 μM).

2.3 Experiment Operation

2.3.1 *Ag/AgCl Electrode Preparation*

The characteristics of the silver/silver chloride (Ag/AgCl) electrode:

1. Reversibility: According to the electrochemical reaction, Ag/AgCl electrode could conduct in two directions.
2. Consuming: After the prolonged current conduction, especially in the high current case, the cathode of AgCl will be consumed, therefore it should be regularly plated.
3. Cl^- dependence: In order to achieve good conductivity, Ag/AgCl electrode must be immersed in a solution containing Cl^- (at least 10 mM).

Both a clean platinum wire and a clean silver wire (after the surface cleaning process, the platinum wire electrode is used as a cathode; after sanding smooth process, the silver electrode is used as an anode) are inserted into the 0.1 M HCl solution, and the electroplating by the external direct current power supply can be controlled by the adjustable resistance. Controlling the current density about 5 mA cm^{-2} for 5 min (at the same current density, there is a positive correlation between the plating time and the AgCl coating thickness. Generally, lower current density and longer plating time will produce the AgCl electrode with better quality), the surface of the silver wire as the anode is coated with AgCl (grayish black). Next, the AgCl electrode can be connected by a conducting wire with the insulating package. AgCl electrode is difficult to preserve, due to the photodecomposition. In addition, the AgCl coating will fall off when it dries. Therefore, after the experiment, the AgCl electrode needs to be washed with the deionized water and then is immersed in KCl solution for next use.

2.3.2 *Ion Transport Measurement System*

As shown in Fig. 2.3, the homemade transmembrane ion transport measurement equipment is a two-electrode system. The platinum electrode is used in the preparation of nanochannels, and the Ag/AgCl electrode is used for the ion transport experiments. Homemade polytetrafluoroethylene (PTFE) electrolyzer is mainly used in the preparation of nanochannels, because PTFE could be well suited for strong acid and alkali (Fig. 2.3a). PTFE three-cell system is used for the parallel etching experiments to get the single channel and multiple channels at the same time (Fig. 2.3b). PTFE two-cell system is individually used in the preparation of the single channel or multiple channels. Homemade plexiglass electrolyzer is used for the ion transport experiments, the advantage is that it can be well observed whether there is a generation of bubbles during the test, which will affect

tests. Figure 2.3c shows the photo of ion transport measurement system. The red line is the output of the positive electrode, and the black line is the negative electrode. The electrode for the output voltage is also a test current electrode. The operating system of the instrument is Keithley Instruments ExceLINX software for the Model 6487, and test voltage range is between -10 and $+10$ V. Keithley 6487 can be used to conduct a variety of testings, such as potentiostatic tests and triangle scanning field tests.

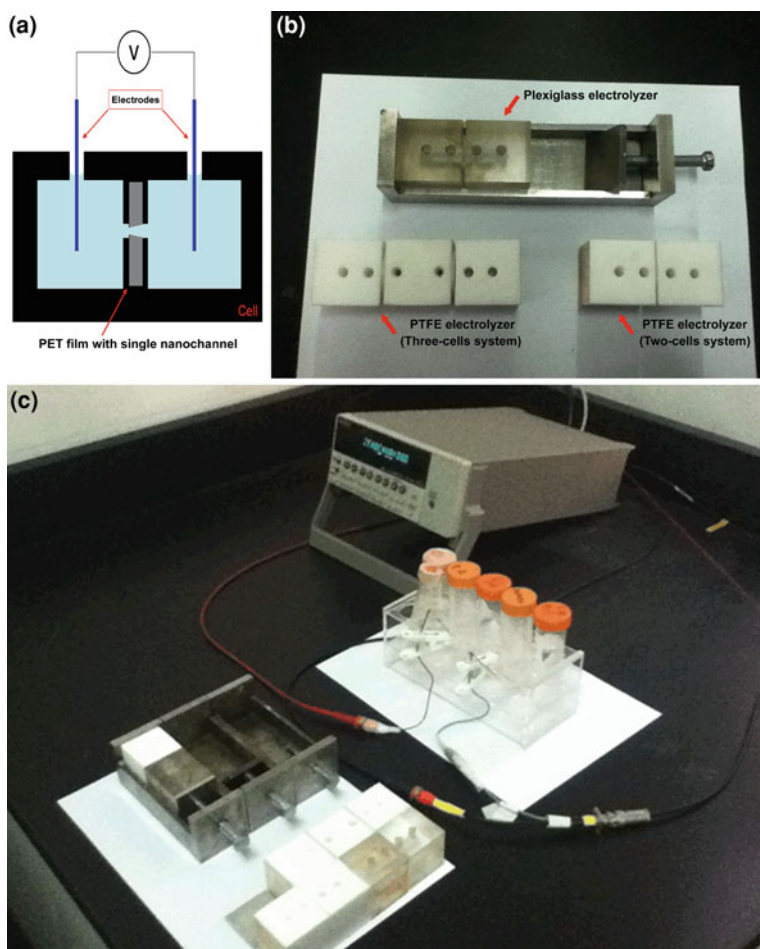


Fig. 2.3 **a** Schematic image of PET film with a conical nanochannel and the cell used for etching and to make all current measurements. **b** The cells. **c** The current measurement apparatus

2.3.3 Preparation of the Conical Shaped Single Nanochannel

The single conical nanochannel investigated here was produced in polymer films using the ion-track-etching technique. This method, which has become well established to create very uniform channel in insulator, is based on the following process (Fig. 1.6): when a swift heavy ion passes through the film, it deposits its energy along its trajectory, thus creating a cylindrical damage zone, i.e., the latent track. By the suitable wet etchants, the damaged material along the track can be removed more quickly than the bulk material, thus developing the tracks into nanochannels. Under the suitable conditions, channels down to a few nanometers in diameter can be produced. During the etching process, negatively charged carboxyl groups, which were attached to flexible polymer chains, were created on the channel surface.

Polyethylene terephthalate (PET, Hostaphan RN 12, Hoechst, thickness 12 μm) is a good candidate to prepare ion track channels with high aspect ratio in free-standing films [37–39]. PET is better suited for applications requiring very narrow channels. Before the chemical etching process, each side of the sample was independently exposed to the UV light for 1 h [36]. To produce a conical nanochannel, etching was performed only from one side, the other side of the cell contains a solution that is able to neutralize the etchant as soon as the channel opens, thus slowing down the further etching process. To additionally stop the etching, the voltage used to monitor the etching process was applied in such a way that the negatively charged ions of the etchant were drawn out of the channel tip (Fig. 1.6). This twofold automatic stopping was mandatory for the controlled production of nanosized channels. The following are the etching and stopping solutions for the etching of PET: 9 M NaOH for etching, 1 M KCl + 1 M HCOOH for stopping. The large opening of the conical nanochannel was called base, while the small opening was called tip. The diameter of the base was estimated from the bulk etch rate measured in the parallel etching experiments (Figs. 2.4, 2.5). The tip diameter was evaluated by the current measurement of the ion conductance of the nanochannel filled with 1 M potassium chloride solution as electrolyte via the following equation:

$$d_{\text{tip}} = \frac{4LI}{\pi k(c)UD} \quad (1)$$

where d_{tip} is the tip diameter, D is the base diameter, and $k(c)$ is the special conductivity of the electrolyte. For 1 M KCl solution at 25 $^{\circ}\text{C}$, $k(c)$ is 0.11173 $\Omega^{-1}\text{cm}^{-1}$. L is the length of the channel, which could be approximated to the thickness of the membrane after chemical etching. U and I are the applied voltage and the measured ion current in the channel conductivity measurement, respectively. In this work, the base diameter was usually several hundred nanometers and the tip diameter was around 20 nm.

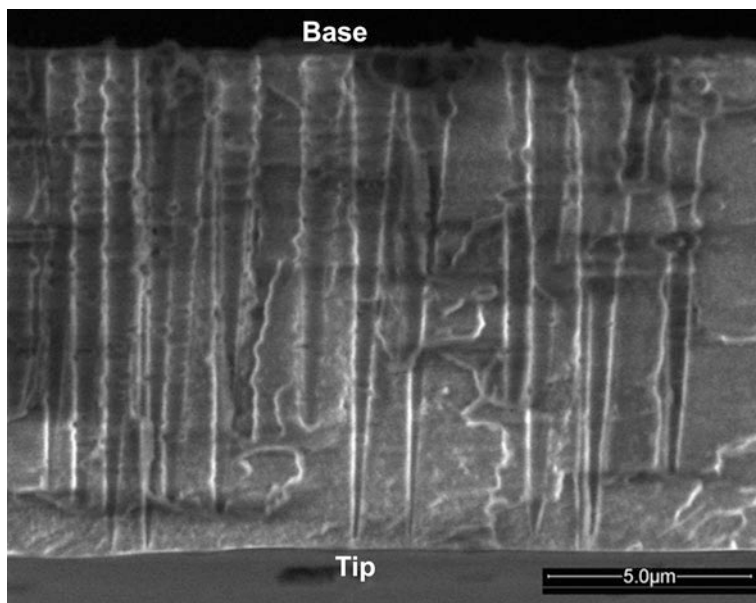


Fig. 2.4 The SEM of the profile of nanochannels, X8000. Scale bar, 5 μm

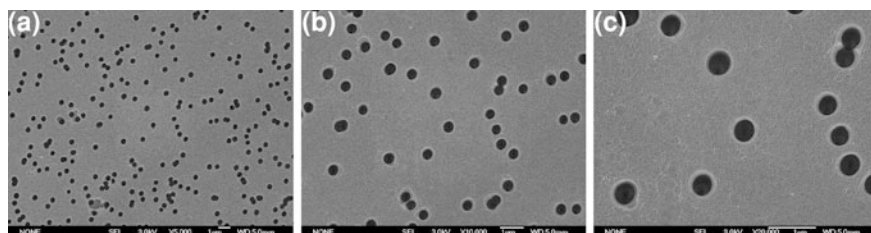


Fig. 2.5 The SEM of base sizes of nanochannels. **a** X5000. **b** X10000. **c** X20000. Scale bars, 1 μm

2.3.4 CD Spectroscopy Measurements

CD spectra were collected on a JASCO J-810 CD spectrometer. CD spectra were measured at 23 $^{\circ}\text{C}$, as maintained by the temperature-control units affiliated to the spectrometers. Wavelength scans were performed between 220 and 320 nm. Quartz cells with a path length of 1 mm were used for DNA and tris solutions. The DNA was dissolved in a Tris buffer solution ($\text{pH} = 7.2$) containing Tris (5 mM) and HCl (4.5 mM) to give the DNA-Tris buffer solution a final concentration of 1 μM in a quartz cell. CD-melting profile recorded at 290 nm. The temperature increased from 10 to 90 $^{\circ}\text{C}$. The average heating rate was about 1 $^{\circ}\text{C}/\text{min}$.

2.3.5 DNA Immobilization

The amino single-stranded G4 DNA (5'-(NH₂)-(CH₂)₆-AAA AAA AAA AGG GTT AGG GTT AGG GTT AGG G (Bodipy493/503)-3') on 5' end (Fig. 2.2) and poly-A DNA(5'-(NH₂)-(CH₂)₆-AAA AAA AAA AAA AAA AAA AAA AAA AAA A (Bodipy493/503)-3') on 5' end were immobilized onto the PET surface and inner channel wall by a two-step chemical reaction, as illustrated in Fig. 2.1. The NHSS ester was formed by exposure of the single-channel contained PET film to an aqueous solution (1 ml MilliQ water, 18.2 MΩ) of 15 mg EDC and 3 mg NHSS for 1 h at 23 °C. These PET-NHSS ester monolayers were reacted for 2 h with a solution of 1 μM amino DNA in MilliQ water at 23 °C. Then, the PET film had been stored for one day in Tris buffer (pH = 7.2, 23 °C) containing Tris (5 mM) and HCl (4.5 mM) before further experiments. The chemical covalent modification in this system is irreversible.

2.3.6 Current Measurement

The nanochannel conductivity and the ion responsive properties of the DNA molecules were studied by measuring ion current through the unmodified nanochannels or DNA-modified nanochannels. Ion current was measured by a Keithley 6487 picoammeter. A single-channel PET membrane was mounted between two chambers of the etching cell mentioned above (Fig. 2.3a). Ag/AgCl electrodes were used to apply a transmembrane potential across the film. Forward voltage was the potential applied on the base side (Fig. 1.6). The main transmembrane potential used in this work was a scanning voltage varied from -2 to +2 V with a 40 s period. Current measurement on the sample treated with Tris solution containing different concentration of alkali metal ions for 1 h before data collection at 23 °C. Each test was repeated five times to obtain the average current value at different voltage.

The previous work has discussed the relationship between positive and negative voltage for the transmembrane potential [8]. It was noticed that ion current signals of the conical nanochannel at low voltages were difficult to distinguish the change of ion transport properties under the little change of ion concentration of the electrolyte solution. Moreover, the electrode might be destroyed at high voltage. Therefore, in this work, the effect of ionic transport properties with different K⁺ concentration on the BNCS is studied at a specific potential in one direction (2 V, anode facing the tip of nanochannel).

2.3.7 XPS Testing

X-ray photoelectron spectroscopy (XPS) analysis was utilized to detect the content of fluorine contained in the fluorescent group at 3' end of the attached DNA molecule, in order to confirm that the DNA was successfully immobilized on PET surface, which was treated by Tris solution after immobilization ($\text{pH} = 7.2$, 296 K). XPS data were obtained by an ESCALab220i-XL electron spectrometer from VG Scientific using 300 W Al K α radiation, and the base pressure was about 3×10^{-9} mbar. The binding energies were referenced to the C1s line at 284.8 eV from adventitious carbon. The XPS test was performed on a separate DNA attached PET surface, which was pretreated by 9 M sodium hydroxide before grafting DNA.

2.4 Results and Discussion

The conformational change of G4 DNA was determined by CD spectroscopy measurements. Control experiments showed that Li^+ had no obvious CD signal within the measured range when the concentration of Li^+ increased from 0 to 10 mM (Fig. 2.6a). As shown in Fig. 2.6b, when the concentration of K^+ increased from 0 to 10 mM, G4 DNA showed a positive peak near 290 nm, a crossover at around 260 nm, and weak negative peaks near 255 and 235 nm, thereby indicating a typical G4 conformation [22, 40]. According to the positive peak near 290 nm, when the concentration of K^+ increased up to 100 mM, the CD signal did not change significantly. It indicated that the major structure of this DNA was G4 conformation within the concentration range from 0 to 10 mM. Considering that the BNCS was realized by folding and unfolding of the G4 DNA, K^+ concentration

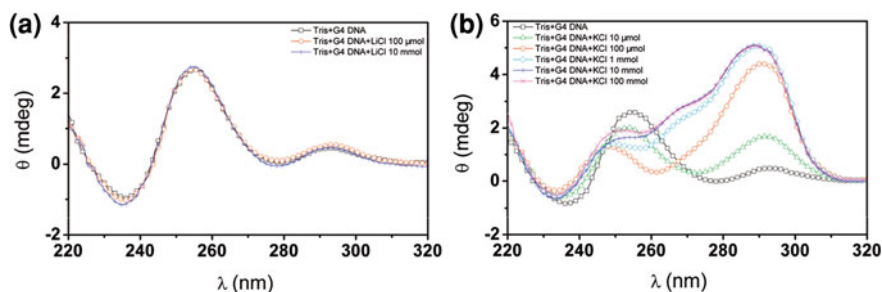


Fig. 2.6 CD spectra of G4 DNA (5'-GGG TTA GGG TTA GGG TTA GGG-3') conformations in the different concentration of alkali metal ions. **a** The concentration of Li^+ of 0 μM (\square , black), 100 μM (\circ , red), 10 mM ($+$, blue). **b** The concentration of K^+ of 0 μM (\square , black), 10 μM (Δ , green), 100 μM (\circ , red), 1 mM (\diamond , cyan), 10 mM ($+$, blue), 100 mM (\times , magenta) in Tris-HCl (5 mM, $\text{pH} 7.2$ at 23 $^{\circ}\text{C}$). Reprinted with the permission from Ref. [1]. Copyright 2009 American Chemical Society

range was determined by G4 conformational change. Thus, this K^+ concentration range was considered as the maximum range for the BNCS current measurements.

In addition, owing to the molecules of fluorin contained in the fluorescent group Bodipy493/503 (green circle, Fig. 2.2) at 3' end of the attached DNA molecule, DNA-modified surface of the PET films were also determined by the X-ray photoelectron spectroscopy analysis. Table 2.4 shows the PET surface without any DNA modification, and PET surface was treated by Tris solution at the same conditions. As the control experiments, it did not contain F1 s signal. Tables 2.5 and 2.6 show the fluorescent groups (Binding Energy of F1 s), indicating the PET surface attached with G4 DNA and poly-A DNA. The PET surface modified by G4 DNA or poly-A DNA did not show obvious difference at F1s signal.

Ion transport properties of the nanochannel were examined by current measurements. Some previous studies related to PET nanochannels have shown that there were two major influencing factors bringing the change of measuring current at the same voltage: ion concentration of the electrolyte solution [38, 41–47] and the effective channel size of the nanochannel [8]. It was assumed that the effective channel size of the nanochannel was determined by two aspects in this BNCS, i.e., the change of physical block and charge density caused by the biomolecular conformational change. In our strategies, the physical block and charge density would change simultaneously because the responsive DNA molecules were highly negatively charged in the pH neutral environment. In the following experiments, these two factors were integrated to investigate the ‘effective channel size’ change, which could more comprehensively explain the new phenomenon in this BNCS. According to the fact that the nanochannel wall [9–11, 48] before and after G4 DNA modification is negatively charged under the neutral conditions, the electrolyte solutions in all the experiments were buffered to a pH value of 7.2 using 5 mM Tris-HCl at 23 °C in order to avoid the influence of pH.

Figure 2.7a shows a positive correlation between Li^+ concentration and the current before G4 DNA modification, which means that the current increased with Li^+ concentration from 0 to 1,500 μM at 2 V (anode facing the tip of nanochannel). After modification, the currents also showed a similar increasing trend but they were lower than that before modification at the same concentration, which could be attributed to the covalently attached DNA molecules that induced a relative reduction of the effective channel size [6]. Whereas the hybridization of the complementary DNA strands with G4 DNA resulted in a sharp decrease in the currents, it still kept an increasing trend.

Table 2.4 The XPS data from PET film before DNA immobilization and treated with Tris solution at pH 7.2 at 23 °C

Name (eV)	Start BE	Peak BE	End BE	Height counts	FWHM eV	Area (P)	CPS.eV	At. %
C1s, 284.8	291.89	284.8	281.2	19890.06	1.89	51689.91		78.11
O1s, 532.2	537.03	532.33	527.9	10597.05	2.97	32997.46		20.88
N1s, 399.5	404.29	399.52	396.89	429.48	0.73	1093.24		1.01

Reprinted with the permission from Ref. [1]. Copyright 2009 American Chemical Society

Table 2.5 The XPS data from PET film after G4 DNA immobilization and treated with Tris solution at pH 7.2 at 23 °C

Name (eV)	Start BE	Peak BE	End BE	Height counts	FWHM eV	Area (P)	CPS.eV	At. %
C1s, 284.8	293.2	284.81	281.34	13131.78	1.74	34589.26		73.73
O1s, 531.9	536.66	531.85	527.6	8545.3	1.91	27173.69		24.25
N1s, 399.7	405.49	399.68	395.37	518.66	1.36	1314.36		1.71
F1s, 689.1	692.55	689	684.69	157.11	0	442.14		0.31

Reprinted with the permission from Ref. [1]. Copyright 2009 American Chemical Society

Table 2.6 The XPS data from PET film after poly-A DNA immobilization and treated with Tris solution at pH 7.2 at 23 °C

Name (eV)	Start BE	Peak BE	End BE	Height counts	FWHM eV	Area (P)	CPS.eV	At. %
C1s, 284.8	293.26	284.79	281.14	10023.19	1.81	27783.84		70.06
O1s, 532.2	536.72	531.93	527.65	8329.17	3.01	26007.9		27.46
N1s, 400.1	405.05	399.89	396.03	364.1	0.09	1263.26		1.95
F1s, 688.8	692.05	688.6	685.13	253.15	0.27	653.34		0.53

Reprinted with the permission from Ref. [1]. Copyright 2009 American Chemical Society

Figure 2.7b shows the current change of the nanochannel via the concentration at different states upon the addition of K^+ . Before G4 DNA modification and after the hybridization, the currents indicated an increasing trend similar to that in Fig. 2.7a. It is worth specially mentioning that there was a remarkable difference after DNA modification. The currents first started to drop with K^+ concentration increasing from 0 to 500 μM , and then the currents changed a little at the concentration range from 500 to 750 μM . Afterward, the concentration further increased from 750 to 1,500 μM , and the currents showed an increasing trend again. This unusual phenomenon could be attributed to the formation of G4 structures that induced the relatively dense packing of DNA molecules on the inner wall of the nanochannel, resulting in an efficient decrease of the effective channel size and thus the current change. These results coincided with the previous studies on the four-stranded i-motif structure [8]. Before the formation of G4 structures, G4 DNA with the single-stranded structure loosely packing on the nanochannel wall could not efficiently reduce the effective channel size, leading to the currents increasing with Li^+ concentration changing from 0 to 1,500 μM (Fig. 2.7a). However, the hybridization of the complementary DNA strands with G4 DNA formed the rigid duplex structure of DNA, and thus created a closely packed arrangement of double-stranded DNA structure that was more stable than G4 structure (Fig. 2.2c). Therefore, G4 DNA conformation could not change with K^+ concentration increasing. This deduction was strongly supported by further experimental data from the CD method.

As shown in Fig. 2.8, after adding the complementary DNA strands, the rigid duplex structures of DNA formed. No change could be observed in CD spectra when K^+ concentration changed from 0 to 1,500 μM , which meant the double-stranded DNA conformation was more stable than that at other states.

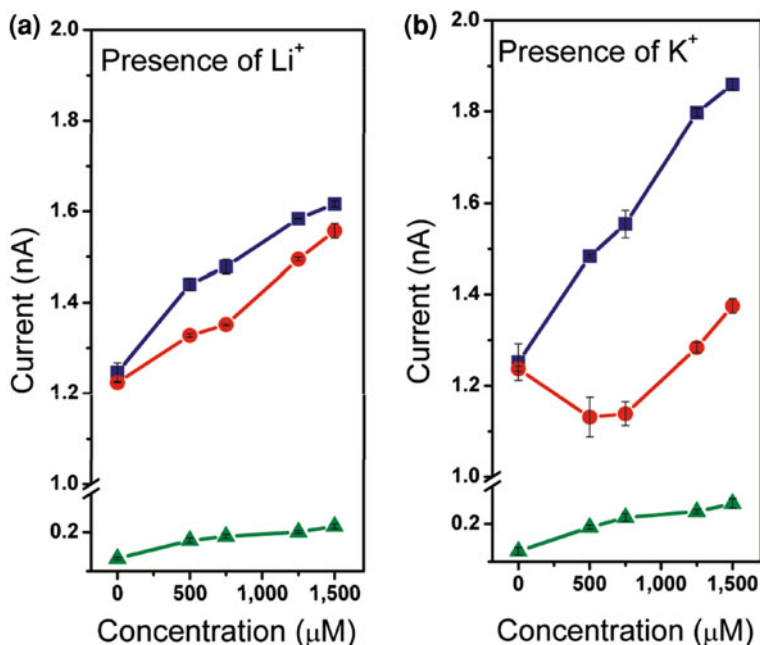


Fig. 2.7 Current-concentration (I - C) properties of a single nanochannel embedded in a PET membrane before and after G4 DNA molecules attached onto the channel wall in Tris-HCl (5 mM, pH = 7.2, at 23 °C). **a** Presence of different Li^+ concentration. **b** Presence of different K^+ concentration. Before G4 DNA modification (■, blue); after G4 DNA modification (●, red); after the addition of the complementary DNA strands (5'-CCC TAA CCC TAA CCC TAA CCC-3') (▲, green). Before modification, the diameter of the tip and base are about 18 and 420 nm, respectively. Reprinted with the permission from Ref. [1]. Copyright 2009 American Chemical Society

To exclude the possible effect of regular DNA of which conformation was not responsive to K^+ , poly-A DNA [8] was selected in this study. From Fig. 2.9, when the system was at its initial state without the alkali metal ions, poly-A DNA showed a negative peak near 247 nm. No change could be observed in CD spectra when the concentration of both K^+ and Li^+ of the buffer solution changed from 0 to 10 mM (G4 conformation appeared at the same K^+ concentration), which indicated there was no distinct conformational change, strongly suggesting that the conformation of poly-A DNA was not responsive to K^+ or Li^+ .

Figure 2.10 shows the current change of a conical nanochannel upon the addition of Li^+ or K^+ before and after poly-A DNA modification under the same conditions, respectively. The ion transport properties of the nanochannel at different states also showed the increasing trend. It was reasonable that poly-A DNA with single-stranded structure loosely packing on the channel wall could not efficiently reduce the effective channel size, leading to the current increase at the ion concentration ranging from 0 to 1,500 μM . These results again verified that the

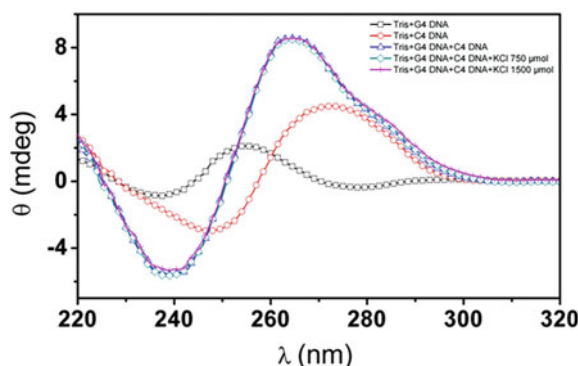


Fig. 2.8 CD spectra of G4 DNA (5'-GGG TTA GGG TTA GGG TTA GGG-3'), the complementary DNA strands (5'-CCC TAA CCC TAA CCC TAA CCC-3') and double-stranded DNA (G4 DNA and the complementary DNA strands). G4 DNA in Tris-HCl, (\square , black); the complementary DNA strands in Tris-HCl, (\circ , red); double-stranded DNA in the different concentration of K^+ ions, (0 μ M, Δ , blue); (750 μ M, \diamond , green); (1500 μ M, $+$, magenta). Reprinted with the permission from Ref. [1]. Copyright 2009 American Chemical Society

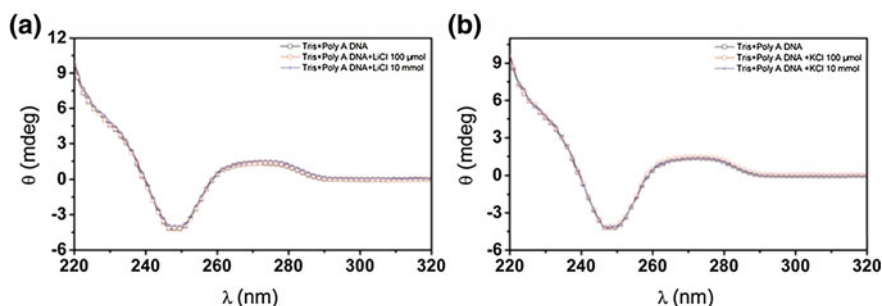


Fig. 2.9 CD spectra of poly-A DNA (5'-AA AAA AAA AAA AAA AAA AAA-3') conformations in the different concentration of alkali metal ions. **a** Li^+ . **b** K^+ . 0 μ M (\square , black), 100 μ M (\circ , red), 10 mM ($+$, blue) in Tris-HCl (5 mM, pH 7.2 at 23 $^{\circ}$ C). Reprinted with the permission from Ref. [1]. Copyright 2009 American Chemical Society

new phenomenon of the current change for K^+ after G4 DNA modification was mainly due to the conformation change of G4 DNA.

In this work, the diameter of the tip around 20 nm was selected to study this BNCS as the optimized channel size discussed in the previous work [8]. As shown in Fig. 2.11, all the nanochannels before modification, of which the tip diameters range from 17 to 24 nm, had the current ratios higher than 1, and exhibited the synthetic nanochannel original property that the current measurements had a positive correlation with alkali metal ion concentration. After the nanochannels were modified with G4 DNA, their current ratios showed the same trend for Li^+ , but a totally different trend for K^+ , which had the current ratios less than 1. Compared to the original nanochannel, the nanochannels modified with poly-A

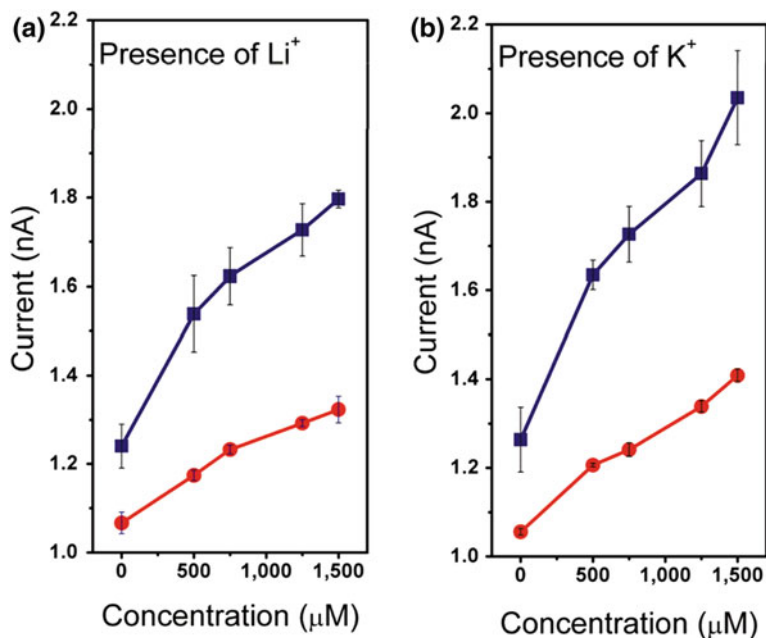


Fig. 2.10 I - C properties of a single nanochannel before and after poly-A DNA molecules attached onto the inner channel wall. **a** Li⁺. **b** K⁺. Before modification (■, blue); after modification (●, red). Before modification, the diameter of the tip and base are about 17 and 400 nm, respectively. Reprinted with the permission from Ref. [1]. Copyright 2009 American Chemical Society

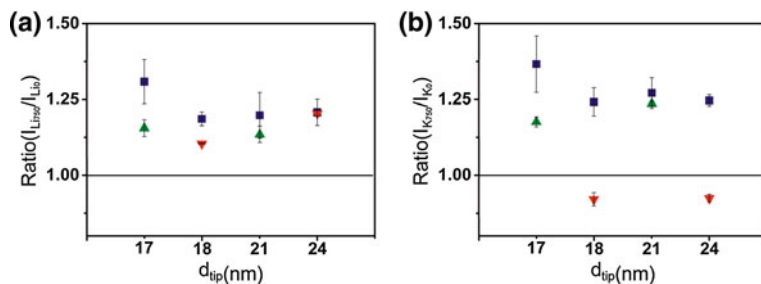


Fig. 2.11 Current ratio of the nanochannels under the absence and presence of 750 μM alkali metal ions before and after DNA modification. **a** Li⁺, **b** K⁺. Before modification (■, blue), after G4 DNA modification (▼, red), after poly-A DNA modification (▲, green). The diameters of the tip and base are about 20 and 400 nm (Sample1, ~17, ~400 nm; Sample2, ~18, 420 nm; Sample3, ~21, ~400 nm; Sample4, ~24, ~410 nm). Reprinted with the permission from Ref. [1]. Copyright 2009 American Chemical Society

DNA showed the similar increasing trend for both Li⁺ and K⁺. Therefore, the conformational change exhibited in G4 DNA molecules indeed contributes to this new phenomenon in the BNCS.

To explore the phenomenon observed in Fig. 2.7b that the currents first decreased and then increased with changes of K^+ concentration, the CD melting method was utilized [21, 23]. It is well-known that G4 DNA melting reveals the ratio of folding and unfolding of G4 DNA, and corresponds to the stability of the G4 structures [21]. Figure 2.12 indicated that the stability of the G4 structures increased with K^+ concentration increasing. The cyan horizontal dot line represents the temperature (T_{et}) for the current measurement. When K^+ concentration exceeded C_{et} (the corresponding concentration of the intersection point between the black curve and the cyan horizontal dot line), the G4 structures became more and more stable with K^+ concentration increasing. With the stability of structures further enhanced, however, the change of the DNA melting rate showed a type of “L” curve (Fig. 2.12, inserts), which means that, for this kind of G4 DNA, K^+ concentration reached a certain level, the stability of the G4 structures nearly kept unchanged. It was found that the most prominent stabilizing of the G4 DNA structure appeared below K^+ concentration of 750 μM .

Based on the above analyses, it can be concluded that enhancing the stability of the G4 structures by increasing K^+ concentration could gradually decrease the effective channel size of the nanochannel within a certain ion concentration ranging from 0 to 750 μM . On the other aspect, K^+ concentration exhibited a positive correlation with the currents change (Fig. 2.7b). Therefore, this new phenomenon of the ion transport properties of the nanochannel modified with G4 DNA was explained by the competition between these two factors, i.e., the stability of G4 structures and ion concentration. To be clearer, when the stability of G4 structures dramatically increased with K^+ concentration increasing, it played a prominent role in changing ion transport properties of the nanochannel by adjusting the effective channel size, while when the increase rate of the stability of G4 structures gradually decreased, the ion concentration started to exert main influence.

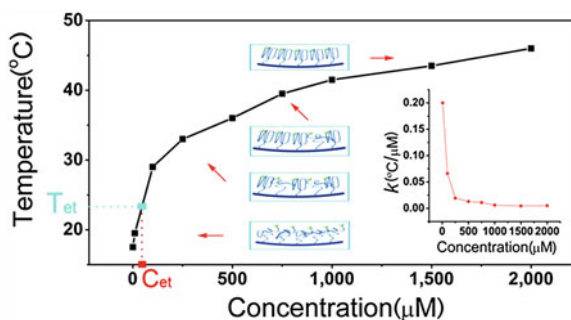


Fig. 2.12 DNA melting—Ion concentration curve of G4 DNA (5'-GGG TTA GGG TTA GGG TTA GGG-3'). The *inserts* represent the stability of G4 structure under different K^+ concentration at the fixed experimental temperature, and influence of different K^+ concentration on the slope of G4 DNA melting and K^+ concentration. Reprinted with the permission from Ref. [1]. Copyright 2009 American Chemical Society

2.5 Conclusions

In summary, we experimentally demonstrate a novel biomimetic nanochannel which can achieve a K^+ response within a certain ion concentration range. The situation of the grafting G4 DNA on a single nanochannel can closely imitate the in vivo condition [21], because the G-rich telomere overhang is attached to the chromosome. Therefore, this artificial system could promote a potential to conveniently study biomolecule conformational change in confined space by the current measurement which is significantly different from the nanopore sequencing [49]. Moreover, such a system as a basic platform could potentially spark further experimental and theoretical efforts to simulate the process of ion transport in living organism and boost the development of bio-inspired intelligent nanochannel apparatus such as biosensors [50, 51], nanofluidic devices [52] and molecular filtration [53].

References

1. Hou X, Guo W, Xia F, Nie FQ, Dong H, Tian Y, Wen LP, Wang L, Cao LX, Yang Y, Xue JM, Song YL, Wang YG, Liu DS, Jiang L (2009) A biomimetic potassium responsive nanochannel: G-Quadruplex DNA conformational switching in a synthetic nanopore. *J Am Chem Soc* 131(22):7800–7805. doi:[10.1021/Ja901574c](https://doi.org/10.1021/Ja901574c)
2. Apel P (2001) Track etching technique in membrane technology. *Radiat Meas* 34(1–6):559–566. doi:[10.1016/s1350-4487\(01\)00228-1](https://doi.org/10.1016/s1350-4487(01)00228-1)
3. Harrell CC, Kohli P, Siwy Z, Martin CR (2004) DNA—Nanotube artificial ion channels. *J Am Chem Soc* 126(48):15646–15647. doi:[10.1021/ja044948v](https://doi.org/10.1021/ja044948v)
4. Kohli P, Harrell CC, Cao ZH, Gasparac R, Tan WH, Martin CR (2004) DNA-functionalized nanotube membranes with single-base mismatch selectivity. *Science* 305(5686):984–986. doi:[10.1126/science.1100024](https://doi.org/10.1126/science.1100024)
5. Schmuhl R, van den Berg A, Blank DHA, ten Elshof JE (2006) Surfactant-modulated switching of molecular transport in nanometer-sized pores of membrane gates. *Angew Chem Int Edit* 45(20):3341–3345. doi:[10.1002/anie.200504579](https://doi.org/10.1002/anie.200504579)
6. Nilsson J, Lee JRI, Ratto TV, Letant SE (2006) Localized functionalization of single nanopores. *Adv Mater* 18(4):427–431. doi:[10.1002/adma.200501991](https://doi.org/10.1002/adma.200501991)
7. Iqbal SM, Akin D, Bashir R (2007) Solid-state nanopore channels with DNA selectivity. *Nat Nanotechnol* 2(4):243–248. doi:[10.1038/nnano.2007.78](https://doi.org/10.1038/nnano.2007.78)
8. Xia F, Guo W, Mao YD, Hou X, Xue JM, Xia HW, Wang L, Song YL, Ji H, Qi OY, Wang YG, Jiang L (2008) Gating of single synthetic nanopores by proton-driven DNA molecular motors. *J Am Chem Soc* 130(26):8345–8350. doi:[10.1021/Ja800266p](https://doi.org/10.1021/Ja800266p)
9. Ali M, Yameen B, Neumann R, Ensinger W, Knoll W, Azzaroni O (2008) Biosensing and supramolecular bioconjugation in single conical polymer nanochannels. facile incorporation of biorecognition elements into nanoconfined geometries. *J Am Chem Soc* 130(48):16351–16357. doi:[10.1021/ja8071258](https://doi.org/10.1021/ja8071258)
10. Ali M, Ramirez P, Mafe S, Neumann R, Ensinger W (2009) A pH-tunable nanofluidic diode with a broad range of rectifying properties. *ACS Nano* 3(3):603–608. doi:[10.1021/nn900039f](https://doi.org/10.1021/nn900039f)
11. Yameen B, Ali M, Neumann R, Ensinger W, Knoll W, Azzaroni O (2009) Single conical nanopores displaying pH-tunable rectifying characteristics. manipulating ionic transport with zwitterionic polymer brushes. *J Am Chem Soc* 131(6):2070–2071. doi:[10.1021/ja8086104](https://doi.org/10.1021/ja8086104)

12. Parkinson GN, Lee MPH, Neidle S (2002) Crystal structure of parallel quadruplexes from human telomeric DNA. *Nature* 417(6891):876–880. doi:[10.1038/nature755](https://doi.org/10.1038/nature755)
13. Patel DJ (2002) Structural biology—a molecular propeller. *Nature* 417(6891):807–808. doi:[10.1038/417807a](https://doi.org/10.1038/417807a)
14. Davis JT (2004) G-quartets 40 years later: From 5'-GMP to molecular biology and supramolecular chemistry. *Angew Chem Int Edit* 43(6):668–698. doi:[10.1002/anie.200300589](https://doi.org/10.1002/anie.200300589)
15. Dittmer WU, Reuter A, Simmel FC (2004) A DNA-based machine that can cyclically bind and release thrombin. *Angew Chem Int Edit* 43(27):3550–3553. doi:[10.1002/anie.200353537](https://doi.org/10.1002/anie.200353537)
16. Alberti P, Bourdoncle A, Sacca B, Lacroix L, Mergny J-L (2006) DNA nanomachines and nanostructures involving quadruplexes. *Org Biomol Chem* 4(18):3383–3391. doi:[10.1039/b605739j](https://doi.org/10.1039/b605739j)
17. Maizels N (2006) Dynamic roles for G4 DNA in the biology of eukaryotic cells. *Nat Struct Mol Biol* 13(12):1055–1059. doi:[10.1038/nsmb1168](https://doi.org/10.1038/nsmb1168)
18. Monchaud D, Yang P, Lacroix L, Teulade-Fichou M-P, Mergny J-L (2008) A metal-mediated conformational switch controls G-quadruplex binding affinity. *Angew Chem Int Edit* 47(26):4858–4861. doi:[10.1002/anie.200800468](https://doi.org/10.1002/anie.200800468)
19. Smargiasso N, Rosu F, Hsia W, Colson P, Baker ES, Bowers MT, De Pauw E, Gabelica V (2008) G-quadruplex DNA assemblies: loop length, cation identity, and multimer formation. *J Am Chem Soc* 130(31):10208–10216. doi:[10.1021/ja801535e](https://doi.org/10.1021/ja801535e)
20. Domene C, Klein ML, Branduardi D, Gervasio FL, Parrinello M (2008) Conformational changes and gating at the selectivity filter of potassium channels. *J Am Chem Soc* 130(29):9474–9480. doi:[10.1021/ja801792g](https://doi.org/10.1021/ja801792g)
21. Zhao Y, Kan ZY, Zeng ZX, Hao YH, Chen H, Tan Z (2004) Determining the folding and unfolding rate constants of nucleic acids by biosensor. Application to telomere G-quadruplex. *J Am Chem Soc* 126(41):13255–13264. doi:[10.1021/ja048398c](https://doi.org/10.1021/ja048398c)
22. Phan AT, Kuryavyi V, Luu KN, Patel DJ (2007) Structure of two intramolecular G-quadruplexes formed by natural human telomere sequences in K^+ solution. *Nucleic Acids Res* 35(19):6517–6525. doi:[10.1093/nar/gkm706](https://doi.org/10.1093/nar/gkm706)
23. Lane AN, Chaires JB, Gray RD, Trent JO (2008) Stability and kinetics of G-quadruplex structures. *Nucleic Acids Res* 36(17):5482–5515. doi:[10.1093/nar/gkn517](https://doi.org/10.1093/nar/gkn517)
24. Forman SL, Fettingner JC, Pieraccini S, Gottarelli G, Davis JT (2000) Toward artificial ion channels: A lipophilic G-quadruplex. *J Am Chem Soc* 122(17):4060–4067. doi:[10.1021/ja9925148](https://doi.org/10.1021/ja9925148)
25. Kaucher MS, Harrell WA, Davis JT (2006) A unimolecular G-quadruplex that functions as a synthetic transmembrane Na^+ transporter. *J Am Chem Soc* 128(1):38–39. doi:[10.1021/ja056888e](https://doi.org/10.1021/ja056888e)
26. Sakai N, Kamikawa Y, Nishii M, Matsuoka T, Kato T, Matile S (2006) Dendritic folate rosettes as ion channels in lipid bilayers. *J Am Chem Soc* 128(7):2218–2219. doi:[10.1021/ja058157k](https://doi.org/10.1021/ja058157k)
27. Lee MPH, Parkinson GN, Hazel P, Neidle S (2007) Observation of the coexistence of sodium and calcium ions in a DNA G-quadruplex ion channel. *J Am Chem Soc* 129(33):10106–10107. doi:[10.1021/ja0740869](https://doi.org/10.1021/ja0740869)
28. Hennig A, Matile S (2008) Detection of the activity of ion channels and pores by circular dichroism spectroscopy: G-quartets as functional CD probes within chirogenic vesicles. *Chirality* 20(9):932–937. doi:[10.1002/chir.20526](https://doi.org/10.1002/chir.20526)
29. Ma L, Melegari M, Colombini M, Davis JT (2008) Large and stable transmembrane pores from guanosine-bile acid conjugates. *J Am Chem Soc* 130(10):2938–2939. doi:[10.1021/ja7110702](https://doi.org/10.1021/ja7110702)
30. Ueyama H, Takagi M, Takenaka S (2002) A novel potassium sensing in aqueous media with a synthetic oligonucleotide derivative. Fluorescence resonance energy transfer associated with guanine quartet-potassium ion complex formation. *J Am Chem Soc* 124(48):14286–14287. doi:[10.1021/ja026892f](https://doi.org/10.1021/ja026892f)

31. He F, Tang YL, Wang S, Li YL, Zhu DB (2005) Fluorescent amplifying recognition for DNA G-quadruplex folding with a cationic conjugated polymer: a platform for homogeneous potassium detection. *J Am Chem Soc* 127(35):12343–12346. doi:[10.1021/ja051507i](https://doi.org/10.1021/ja051507i)
32. He F, Tang YL, Yu MH, Feng F, An LL, Sun H, Wang S, Li YL, Zhu DB, Bazan GC (2006) Quadruplex-to-duplex transition of G-rich oligonucleotides probed by cationic water-soluble conjugated polyelectrolytes. *J Am Chem Soc* 128(21):6764–6765. doi:[10.1021/ja058075w](https://doi.org/10.1021/ja058075w)
33. Huang C-C, Chang H-T (2008) Aptamer-based fluorescence sensor for rapid detection of potassium ions in urine. *Chem Commun* 12:1461–1463. doi:[10.1039/b718752a](https://doi.org/10.1039/b718752a)
34. Phan AT, Mergny JL (2002) Human telomeric DNA: G-quadruplex, i-motif and watson-crick double helix. *Nucleic Acids Res* 30(21):4618–4625. doi:[10.1093/nar/gkf597](https://doi.org/10.1093/nar/gkf597)
35. Sen D, Gilbert W (1990) A sodium-potassium switch in the formation of 4-stranded G4-DNA. *Nature* 344(6265):410–414. doi:[10.1038/344410a0](https://doi.org/10.1038/344410a0)
36. Apel PY, Korchev YE, Siwy Z, Spohr R, Yoshida M (2001) Diode-like single-ion track membrane prepared by electro-stopping. *Nucl Instrum Meth Phys Res Sect B Beam Interact Mater Atoms* 184(3):337–346. doi:[10.1016/s0168-583x\(01\)00722-4](https://doi.org/10.1016/s0168-583x(01)00722-4)
37. Siwy Z, Apel P, Baur D, Dobrev DD, Korchev YE, Neumann R, Spohr R, Trautmann C, Voss KO (2003) Preparation of synthetic nanopores with transport properties analogous to biological channels. *Surf Sci* 532:1061–1066. doi:[10.1016/s0039-6028\(03\)00448-5](https://doi.org/10.1016/s0039-6028(03)00448-5)
38. Harrell CC, Siwy ZS, Martin CR (2006) Conical nanopore membranes: Controlling the nanopore shape. *Small* 2(2):194–198. doi:[10.1002/sml.200500196](https://doi.org/10.1002/sml.200500196)
39. Wharton JE, Jin P, Sexton LT, Horne LP, Sherrill SA, Mino WK, Martin CR (2007) A method for reproducibly preparing synthetic nanopores for resistive-pulse biosensors. *Small* 3(8):1424–1430. doi:[10.1002/sml.200700106](https://doi.org/10.1002/sml.200700106)
40. Xu Y, Noguchi Y, Sugiyama H (2006) The new models of the human telomere d AGGG (TTAGGG)(3) in K⁺ solution. *Bioorg Med Chem* 14 (16):5584–5591. doi:[10.1016/j.bmc.2006.04.033](https://doi.org/10.1016/j.bmc.2006.04.033)
41. Siwy Z, Fulinski A (2002) Fabrication of a synthetic nanopore ion pump. *Phys Rev Lett* 89 (19). doi:198103 [10.1103/PhysRevLett.89.198103](https://doi.org/10.1103/PhysRevLett.89.198103)
42. Kumar S, Chakarvarti SK (2003) On the preparation and asymmetric electric transport behavior of conical channels in polyethylene terephthalate. *Radiat Meas* 36(1–6):757–760. doi:[10.1016/s1350-4487\(03\)00241-5](https://doi.org/10.1016/s1350-4487(03)00241-5)
43. Siwy Z, Apel P, Dobrev D, Neumann R, Spohr R, Trautmann C, Voss K (2003) Ion transport through asymmetric nanopores prepared by ion track etching. *Nucl Instrum Methods Phys Res Sect B Beam Interact Mater Atoms* 208:143–148. doi:[10.1016/s0168-583x\(03\)00884-x](https://doi.org/10.1016/s0168-583x(03)00884-x)
44. Schiedt B, Healy K, Morrison AP, Neumann R, Siwy Z (2005) Transport of ions and biomolecules through single asymmetric nanopores in polymer films. *Nucl Instrum Meth Phys Res Sect B Beam Interact Mater Atoms* 236:109–116. doi:[10.1016/j.nimb.2005.03.265](https://doi.org/10.1016/j.nimb.2005.03.265)
45. Siwy Z, Kosinska ID, Fulinski A, Martin CR (2005) Asymmetric diffusion through synthetic nanopores. *Phys Rev Lett* 94(4). doi:[10.1103/PhysRevLett.94.048102](https://doi.org/10.1103/PhysRevLett.94.048102)
46. Siwy ZS (2006) Ion-current rectification in nanopores and nanotubes with broken symmetry. *Adv Funct Mater* 16(6):735–746. doi:[10.1002/adfm.200500471](https://doi.org/10.1002/adfm.200500471)
47. Powell MR, Sullivan M, Vlasiouk I, Constantin D, Sudre O, Martens CC, Eisenberg RS, Siwy ZS (2008) Nanoprecipitation-assisted ion current oscillations. *Nat Nanotechnol* 3 (1):51–57. doi:[10.1038/nnano.2007.420](https://doi.org/10.1038/nnano.2007.420)
48. Siwy Z, Heins E, Harrell CC, Kohli P, Martin CR (2004) Conical-nanotube ion-current rectifiers: the role of surface charge. *J Am Chem Soc* 126(35):10850–10851. doi:[10.1021/ja047675c](https://doi.org/10.1021/ja047675c)
49. Branton D, Deamer DW, Marziali A, Bayley H, Benner SA, Butler T, Di Ventra M, Garaj S, Hibbs A, Huang X, Jovanovich SB, Krstic PS, Lindsay S, Ling XS, Mastrangelo CH, Meller A, Oliver JS, Pershin YV, Ramsey JM, Riehn R, Soni GV, Tabard-Cossa V, Wanunu M, Wiggin M, Schloss JA (2008) The potential and challenges of nanopore sequencing. *Nat Biotechnol* 26(10):1146–1153. doi:[10.1038/nbt.1495](https://doi.org/10.1038/nbt.1495)
50. Choi Y, Baker LA, Hillebrenner H, Martin CR (2006) Biosensing with conically shaped nanopores and nanotubes. *Phys Chem Chem Phys* 8(43):4976–4988. doi:[10.1039/b607360c](https://doi.org/10.1039/b607360c)

51. Martin CR, Siwy ZS (2007) Learning nature's way: biosensing with synthetic nanopores. *Science* 317(5836):331–332. doi:[10.1126/science.1146126](https://doi.org/10.1126/science.1146126)
52. Huh D, Mills KL, Zhu X, Burns MA, Thouless MD, Takayama S (2007) Tuneable elastomeric nanochannels for nanofluidic manipulation. *Nat Mater* 6(6):424–428. doi:[10.1038/nmat1907](https://doi.org/10.1038/nmat1907)
53. Savariar EN, Krishnamoorthy K, Thayumanavan S (2008) Molecular discrimination inside polymer nanotubules. *Nat Nanotechnol* 3(2):112–117. doi:[10.1038/nnano.2008.6](https://doi.org/10.1038/nnano.2008.6)

Bio-inspired Asymmetric Design and Building of
Biomimetic Smart Single Nanochannels

Hou, X.

2013, XIII, 127 p. 78 illus., 67 illus. in color., Hardcover

ISBN: 978-3-642-38049-5